Materials Science and Engineering C 29 (2009) 2333–2339

Contents lists available at ScienceDirect

Materials Science and Engineering C

journal homepage: www.elsevier.com/locate/msec

A study on the structure and mechanical behavior of the *Terrapene carolina* carapace: A pathway to design bio-inspired synthetic composites

H. Rhee [a,*], M.F. Horstemeyer [a,b], Y. Hwang [a], H. Lim [c], H. El Kadiri [a], W. Trim [a,b]

[a] Center for Advanced Vehicular Systems, Mississippi State University, Mississippi State, MS 39762-5405, USA
[b] Department of Mechanical Engineering, Mississippi State University, Mississippi State, MS 39762-9552, USA
[c] Department of Mathematics and Statistics, Mississippi State University, Mississippi State, MS 39762-9715, USA

ARTICLE INFO

Article history:
Received 3 December 2008
Received in revised form 29 May 2009
Accepted 10 June 2009
Available online 21 June 2009

Keywords:
Turtle shell
Carapace
Multiscale hierarchical structure
Sandwich composite
Bony exterior
Foam-like interior

ABSTRACT

The multiscale structure, materials properties, and mechanical responses of the turtle shell (*Terrapene carolina*) were studied to understand the fundamental knowledge of naturally occurring biological penetrator-armor systems. The structure observation and chemical analysis results revealed that the turtle shell carapace comprises a multiphase sandwich composite structure of functionally graded material having exterior bone layers and a foam-like bony network of closed-cells between the two exterior bone layers. Although the morphology was quite different, the exterior bone layers and interior bony network possessed comparable hardness and elastic modulus values of ~1 GPa and ~20 GPa, respectively. Compression and flexure test results showed a typical nonlinear deformation behavior recognizant of man-made foams. The mechanical test results revealed that the interior closed-cell foam layer plays a significant role on the overall deformation behavior of the turtle shell. The finite element analysis simulation results showed comparable agreement with the actual experimental test data. This systematic study could provide fundamental understanding for structure-property phenomena and biological pathways to design bio-inspired synthetic composite materials.

© 2009 Elsevier B.V. All rights reserved.

1. Introduction

Biological materials, particularly structural composite materials, have occupied the attention of many researchers in the recent years due to their novel hierarchical structures and remarkable mechanical properties that are far beyond their component properties and synthetic counterparts [1–4]. Since composite materials can attain unique combinations of mechanical properties, some biological composite structures have been used to resist penetration, *e.g.* a turtle shell. Such distinctive mechanical properties of biological composite materials are the consequences of their organization in terms of composition and structure. In general, they comprise both organic and inorganic components in their complexity, and these structures are hierarchically organized at the nano-, micro-, and meso-scale levels unlike those found in man-made counterpart materials [1].

In nature, a hierarchy of different composite structures exists for various animals. These natural (biological) armor systems are designed to resist different types of penetration events and as such have similarities and differences. Several studies on the structures and mechanical responses of different biological composite materials have been extensively reported in the literature [1–22]. For example, the microstructure and deformation behavior of a crab or lobster cuticle have been studied by Raabe et al. [15–17], and those of mollusk shells have been investigated by Katti et al. [5–11]. In addition, those of abalone shells have been studied by Meyers et al. [1–4]. They have recently worked on the toucan beak as well [18,21]. The material modeling and associated finite element analysis (FEA) regarding the aforementioned biological materials can also be found in the literature [5–8,18,22]. In our study, we are exclusively focusing on the structures, materials properties, and mechanical behavior of the turtle shell, which to the authors' knowledge has not been studied in this fashion.

Turtles are reptiles of the order *Testudines*, most of whose body is shielded by a special bony or cartilaginous shell developed from their ribs [23]. The turtle shell is usually a fairly firm and rigid structure, although in a few cases, such as the soft-shelled turtles, this covering is softer. Divided into two parts, the turtle shell's upper part is known as the *carapace*, and the lower part is called the *plastron*. The turtle's vital organs are well protected by these dorsal and ventral shields [23–25]. These two parts are strongly connected together for structural support by bony bridges that are located between the front and hind limbs on each side of the body. The strength and rigidity of the turtle shell itself results from an inner bony casing of fused plates, which in turn are covered by a horny shield made of keratin *scutes* or *laminae*.

Although the turtle shell carapace possesses superior armor behavior against environmental threats, their structure and mechanical responses surprisingly have not been studied. The main objective of the present study is to quantify the impact capability of the turtle shell based on the materials, geometric characteristics, and the multiscale

* Corresponding author. Tel.: +1 662 3259221; fax: +1 662 3255433.
E-mail address: hrhee@cavs.msstate.edu (H. Rhee).

0928-4931/$ – see front matter © 2009 Elsevier B.V. All rights reserved.
doi:10.1016/j.msec.2009.06.002

microstructure-property relations. Since no structure-property relations have been analyzed on the turtle shell, there exists a lack of experimental database of such biological structural material. Moreover, there is no systematic research on this biological structure to understand structure-property phenomena and biological pathways to create bio-inspired synthetic materials. Therefore, a comparison–contrasting study of the structure–property relations between the turtle shell and other biological structural materials could provide understanding for novel bio-inspired safety system design methodologies.

2. Experimental procedures

Multiscale structure and mechanical properties were quantified under nano-, micro-, meso-, and macro-scales by using the turtle shell obtained from the natural death of a box turtle (*Terrapene carolina*). The structure of the turtle shell was investigated by using an optical microscope and a scanning electron microscope (SEM). The top and bottom surfaces and cross-section of the turtle shell carapace were sectioned by using a diamond saw and prepared for microstructure observations. Sectioned specimens were cleaned by an ultrasonic cleaner and then mounted in epoxy by using a cold mount technique to minimize the detrimental effects during preparation of these biological samples. Mounted samples were then sputter-coated with gold and examined under a SUPRA-40 field emission gun (FEG)-SEM made by CarlZeiss SMT Ltd.

Mechanical tests in this research included nano- and micro-indentations, quasi-static compression, and bending tests. Nano-indentation tests were conducted to gain micromechanical properties of various phases found in the turtle shell carapace (*e.g.* outer, inner, and side surfaces of the shell). These tests were performed with a TriboIndenter® from Hysitron Incorporated at room temperature using a Berkovich type indenter under load control that included a 20 s loading segment, a 2 s constant-load hold time, and a 20 s unloading segment. The loading and unloading rates of such tests were 450 μN/s. Strain rate effects were not studied in this work but have been included in a forthcoming paper. Hence, for this particular applied rate, the hardness and elastic modulus at the region of indenting point were determined. SEM images were taken and characterized for most of the indents made to obtain additional information regarding the deformation and fracture processes associated with indentation. Micro-indentation tests were carried out to obtain more global information on the side surfaces of the turtle shell carapace using a Vickers hardness tester made by LECO Corporation. These tests were conducted at room temperature using a pyramidal diamond tip and a load of 25 gf was used throughout.

Quasi-static compression tests were conducted by using an Instron 5882 electromechanical test apparatus and the maximum load capacity of the machine and the load cell was 100 kN. All tests were carried out at room temperature with various strain rates ranged from 10^{-4} to 10^{0} s^{-1} by using coupon specimens detached from the turtle shell carapace.

Flexure tests by using a three-point bending set-up were performed using the aforementioned Instron machine at room temperature with a cross-head speed of 0.5 mm/min. The strain was measured with a linear variable displacement transducer (LVDT) due to the limitations on the specimen geometry and the minimum gage size of available extensometers. In addition, the foil strain gages were directly attached to the top and underneath sides of the coupon specimen, and the strain histories at specific locations were recorded. The recorded signals were analyzed using NI-DAQmx software from National Instruments. The specimens were created according to ASTM D790 and cut as longitudinal and transverse directions of the turtle shell carapace.

Finite element analyses (FEA) of the three-point bending tests were performed using a commercial code, ABAQUS, based on the material properties given from the indentation tests. The turtle shell carapace is essentially a sandwich composite material comprising three distinct regions of the outer shell, inner core, and outer shell. The two outer shells act as a face sheet of the sandwich composite, and the material between two outer shells behaves as a soft core material. Therefore, two modeling approaches were considered to simulate the

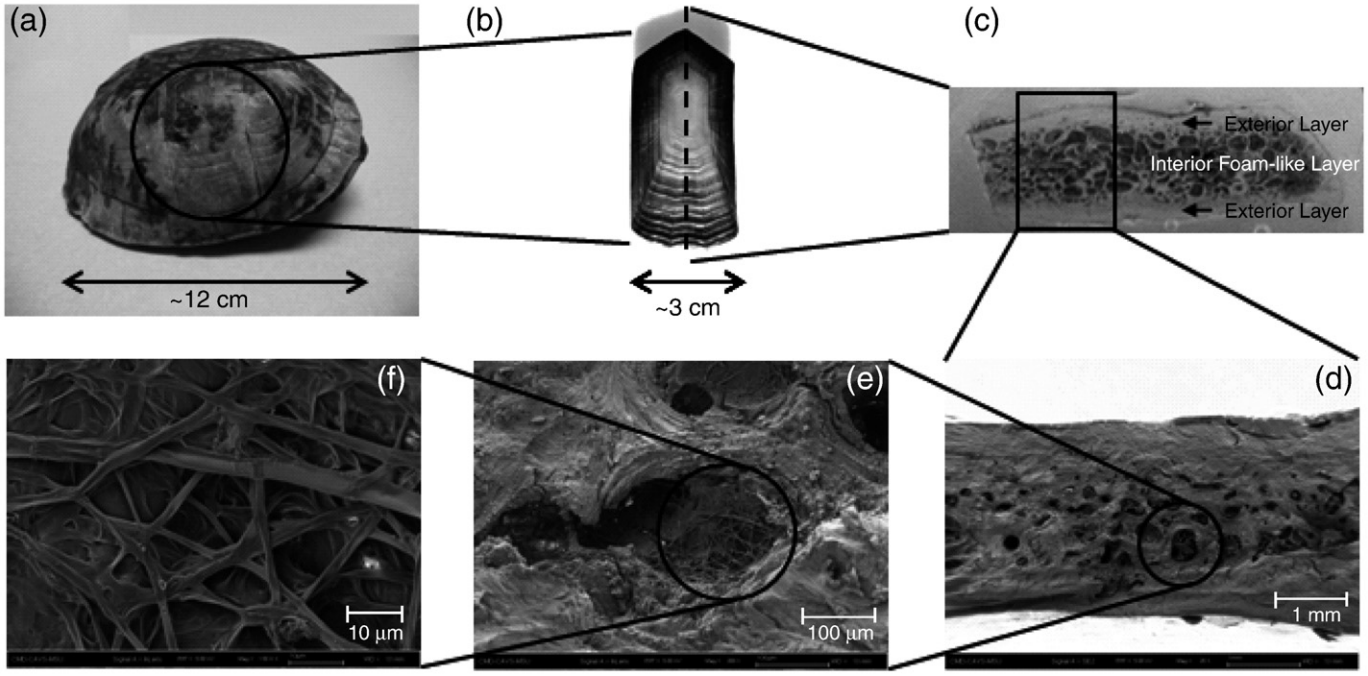

Fig. 1. Multiscale hierarchy and structure of the turtle shell; (a) a morphology of the turtle shell carapace, (b) a costal scute showing the successive growth pattern, (c) a cross-sectional view of the carapace showing composite layers, (d) an SEM micrograph of a fracture surface, (e) an SEM micrograph of a cell structure, and (f) an SEM micrograph of a fibrous structure inside of the cell.

three-point bend tests to better capture the physical responses of the turtle shell structure. The first approach employed an eight-node shell element through-the-thickness direction with a composite lay-up to take account for the outer shells and the soft core of the turtle shell. This approach is widely used in composite materials with a certain range of thickness and similar material properties in each laminate [26–28]. A second approach employed a three-discrete layer that had two eight-node shell elements for the outer shells and a twenty-node brick element for the inner core between the two outer shells in the through-the-thickness direction. This method is typically used for sandwich composites with a relatively soft core material that includes hard outer materials.

3. Results and discussion

Structure observations on the turtle shell revealed a multiphase composite material that is arranged by a multiscale hierarchy. Such a multiscale hierarchical structure of the turtle shell carapace is depicted in Fig. 1. The turtle shell comprises a series of connected individual plates covered with a layer of horny keratinized scutes (Fig. 1a–b). The scutes are made up of a fibrous protein called keratin that also comprises the scales of other reptiles [5]. These scutes overlap the seams between the shell bones and serve to reinforce the overall protection to the shell. The carapace is made of a sandwich composite structure of functionally graded material (FGM) having relatively denser exterior layers and an interior fibrous foam-like layer (Fig. 1c–d). SEM micrographs clearly revealed such fibrous structure inside of the cell (Fig. 1e–f).

The internal structure of the turtle shell was nondestructively observed by using an X-ray computed tomography (CT) and obtained images are provided in Fig. 2. The X-ray CT was carried out by using a v|tome|x by phoenix|x-ray. The X-ray CT images clearly showed that the pores within the interior foam-like layer of the turtle shell carapace were closed-cell type and randomly distributed. In addition, the results obtained from the in-house image analyzer software revealed that the porosity levels of the relatively denser exterior, interior foam-like layer, and whole turtle shell carapace including all three layers were 6.86%, 65.5%, and 48.9%, respectively.

Figs. 3 and 4 show the microstructure observation and chemical analysis results obtained from various surfaces of the turtle shell. Three different layers of the outermost keratin layer, right underneath the keratin layer, and the inside surface of the turtle shell carapace were observed and analyzed by using an SEM and an energy dispersive X-ray (EDX) spectroscopy technique, respectively. These layers have different surface microstructures and chemical compositions. The EDX analysis showed that the outermost keratin layer mainly consists of carbon (C), oxygen (O), nitrogen (N), and sulfur (S) that are main constituents of the protein. The result is not surprising since the keratins are a family of fibrous structural proteins, also called *scleroproteins*. Unlike the outermost keratin layer, right underneath the keratin layer and the inside surface of the turtle shell carapace contained abundant additional minerals as indicated by the presence of calcium (Ca, 15–20 wt.%), phosphorous (P, 7–10 wt.%), sodium (Na), chlorine (Cl), and magnesium (Mg) that are known to be main components of the bone.

The microstructures and chemical analysis results obtained from different locations of the fracture surfaces of the turtle shell carapace are provided in Figs. 5 and 6. The chemical compositions obtained from the exterior layers and the network (*e.g.* closed-cell wall) region within the foam-like interior layer were quite similar to those can be found in Fig. 4b–c. The fibers inside of the closed-cell also showed an accordant chemical composition (Fig. 6b), which implies that they include "bony" fibers. The microstructure observation and chemical analysis results obtained from various locations of the turtle shell clearly revealed that the turtle shell carapace is made of a sandwich composite structure having exterior lamellar bone layers and an interior bony network of closed-cell fibrous foam layer.

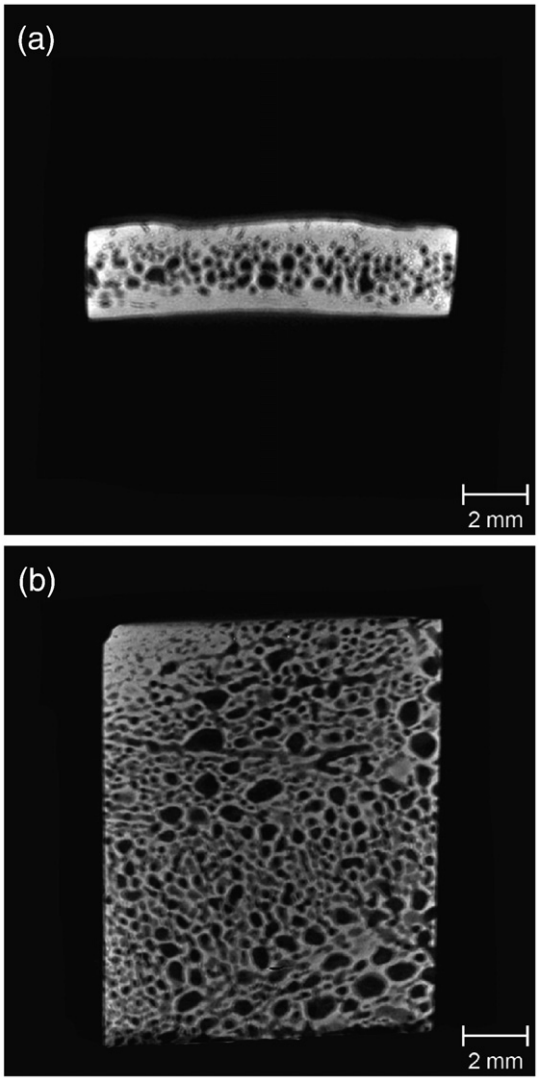

Fig. 2. (a) A side sectional view and (b) a top sectional view of the turtle shell carapace coupon obtained from X-ray CT single slice scan showing randomly distributed closed-cell pores within the foam-like interior layer.

Experimental results obtained from the nano- and micro-indentation tests on the side surfaces of the turtle shell carapace are provided in Fig. 7. The results showed that the exterior layers and interior bony closed-cell walls possess comparable hardness and modulus values. Hardness and elastic modulus values obtained from the nano-indentation tests ranged from 0.8–1.1 GPa and 18.3–24.8 GPa, respectively; whereas, the average hardness value obtained from the Vickers hardness tests was about Hv100 that corresponds to 0.98 GPa. There were small variations in hardness and elastic modulus values from experiments due to the roughness of the specimen. The nano-indentation test results reflect highly localized micromechanical properties that may contain porous or impurities in its texture. Since the regions of indentation are so small that local impurities or defects can induce uncertainties in the measurements. This effect is minimized under Vickers hardness test set-up and the exterior layers and closed-cell walls within an interior layer possessed comparable hardness values.

For quasi-static compression tests, two different types of coupon specimens including all three layers and then only a bony exterior layer were prepared. The effect of strain rate on the mechanical

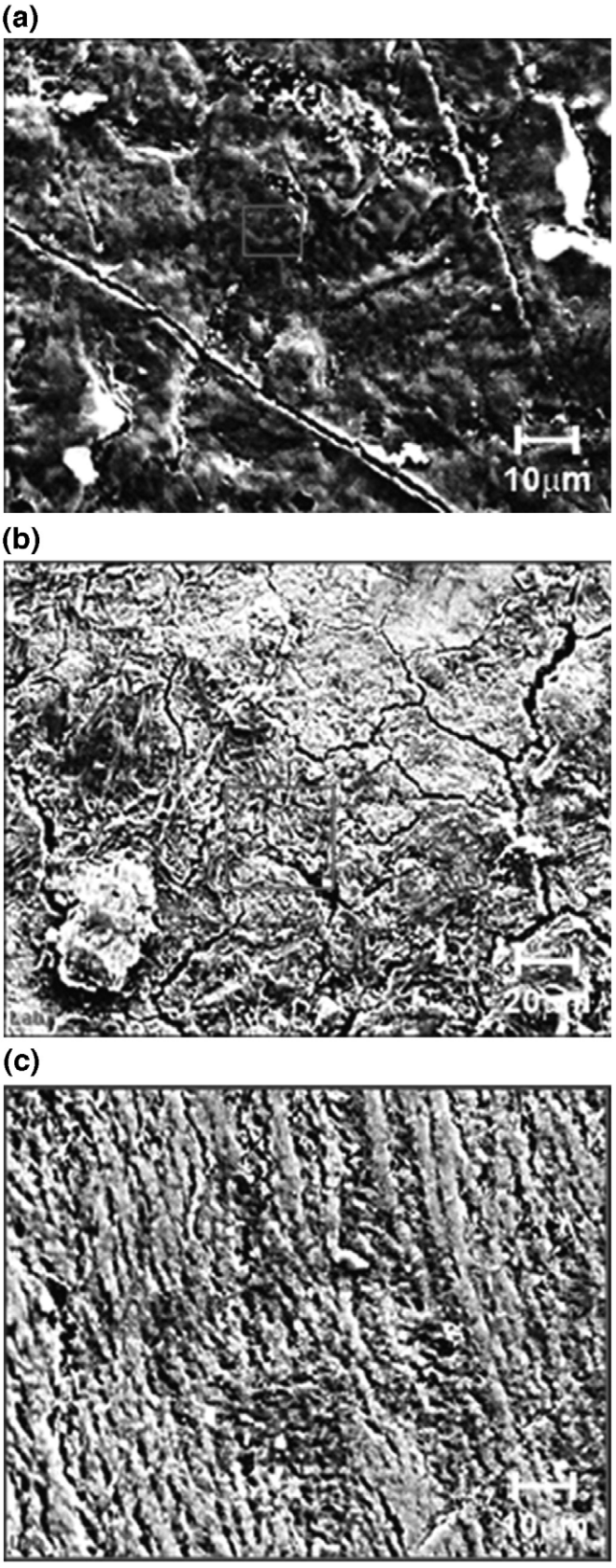

Fig. 3. SEM micrographs obtained from different surfaces of the turtle shell carapace; (a) the outermost keratin layer, (b) underneath the keratin layer, and (c) inside surface.

behavior of the turtle shell was compared with respect to the different density levels and the raw data obtained from the tests is illustrated in Fig. 8a. The lower five curves (represented by lines with symbols) were obtained from the test specimens including all three layers (two exterior and an interior layers); whereas the upper six curves were

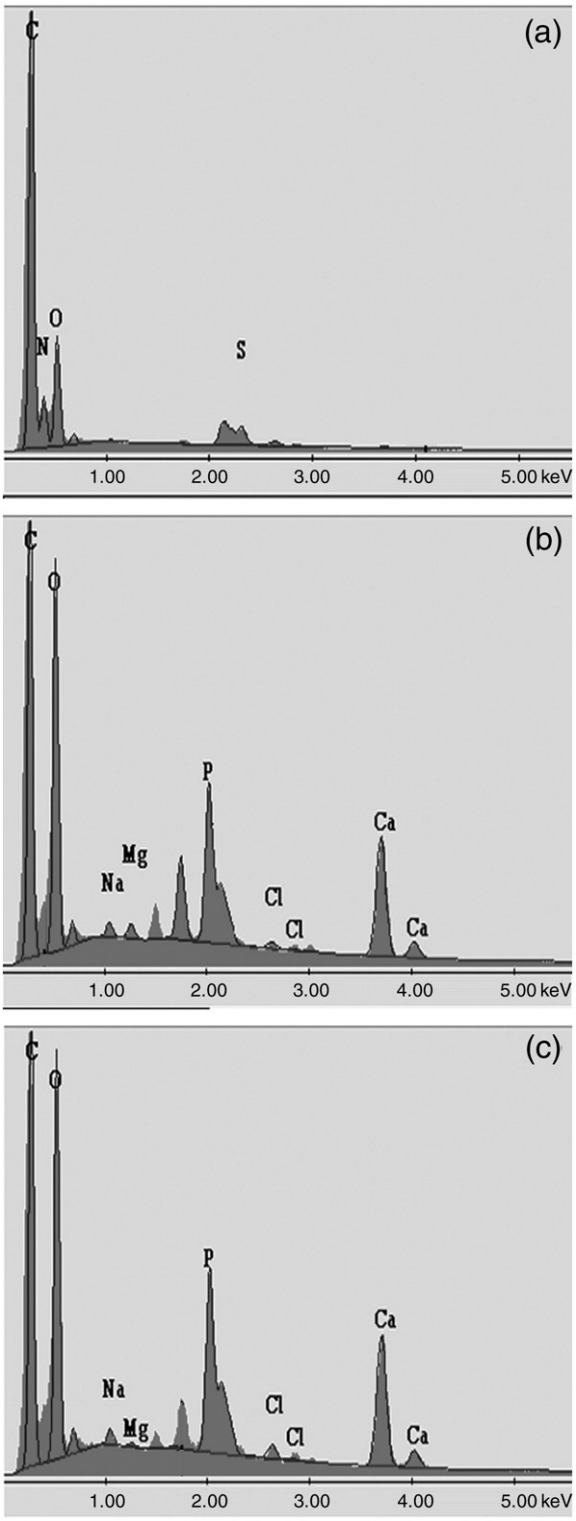

Fig. 4. Chemical analysis results obtained from different surfaces of the turtle shell carapace; (a) the outermost keratin layer, (b) underneath the keratin layer, and (c) inside surface.

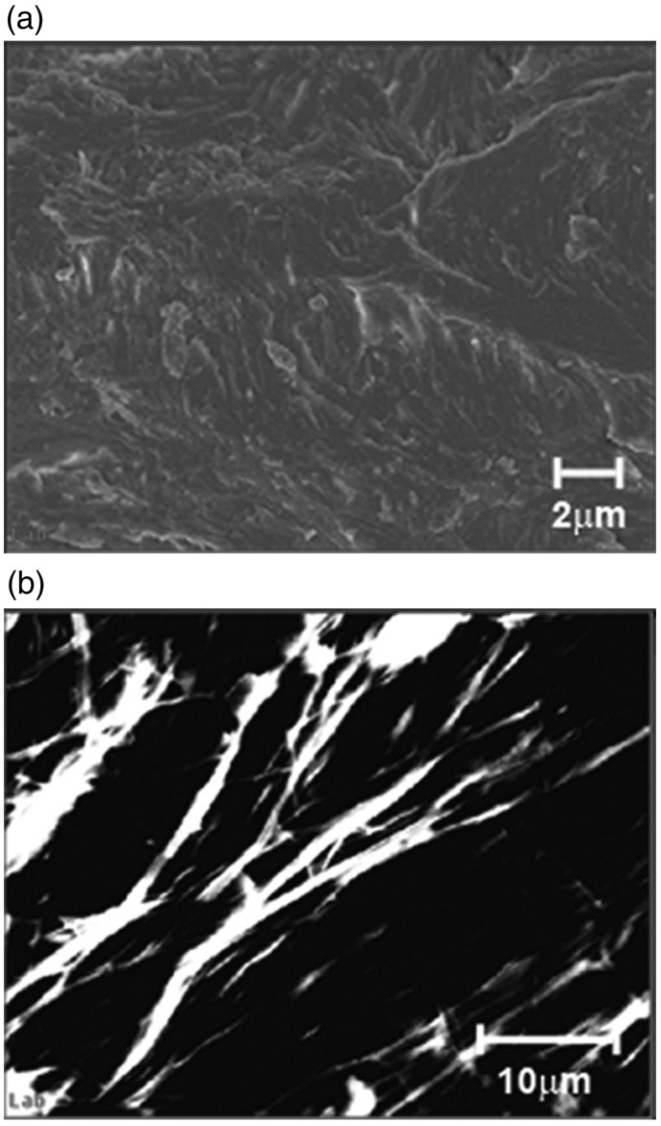

Fig. 5. SEM micrographs obtained from the fracture surface of the turtle shell carapace; (a) bony layers and (b) inside of the closed-cell (fibers).

obtained from the specimens only containing a relatively denser exterior layer. Top three curves (in symbols) among those six curves were obtained from thinner specimens and the bottom three curves (in lines) represent thicker specimens. The thickness difference between those two regimes was about 15%. The favorable deformation mechanism of the turtle shell carapace under quasi-static compression test conditions can be explained by importing that of synthetic foams and/or honeycombs since fundamental structures of the test specimens are similar to those of such cellular solids. At small strains, the specimens were deformed in a linear elastic manner due to the cell wall bending [29]. Soon after the initial linear elastic deformation, a plateau of deformation was reached, because of the buckling of the cell walls. After such a plateau of deformation, another period of linear deformation was proceeded since a densification occurred resulting in a rapid increase of compressive stress. When comparing the specimens containing the exterior region only, the thicker specimens showed a similar deformation yet much weaker behavior than those can be observed in the specimens including all three layers; whereas the thinner specimens showed almost a linear compressive deformation behavior simply because of the density and structure differences. Most of discernible pores within exterior layer are distributed near the region between the exterior layer and interior foam-like layer. Fig. 8b provides the comparison of specific energy absorption obtained from the quasi-static compression test results (Fig. 8a). Density and porosity levels of the test specimens were already considered in this normalized data. The energy absorption ability of the turtle shell carapace increased with increasing strain rate for a given density level. The composite layers including all three layers showed better energy absorption ability compared to the exterior layer for any given strain rate. In addition, such composite layers possessed a considerable amount of plateau of deformation that is a model index of good energy absorbing materials. The combining information of these two plots in Fig. 8 is very important to design the optimum energy absorbing composite material. For example, composite foam materials can be tailored to give the best combination of properties for a given package by choosing the right combination of the cell wall materials, relative density, reinforcement phases, and so on.

Flexure tests using a three-point bending mode were carried out on a coupon specimen sampled from the turtle shell carapace and compared with finite element simulation results. The specimens were cut as longitudinal and transverse directions of the turtle shell, and no apparent difference in the stress–strain relations with respect to the different orientations were noted. The flexural stress (σ_f), flexural strain (ε_f), and Young's modulus in bending (E_B) for the rectangular

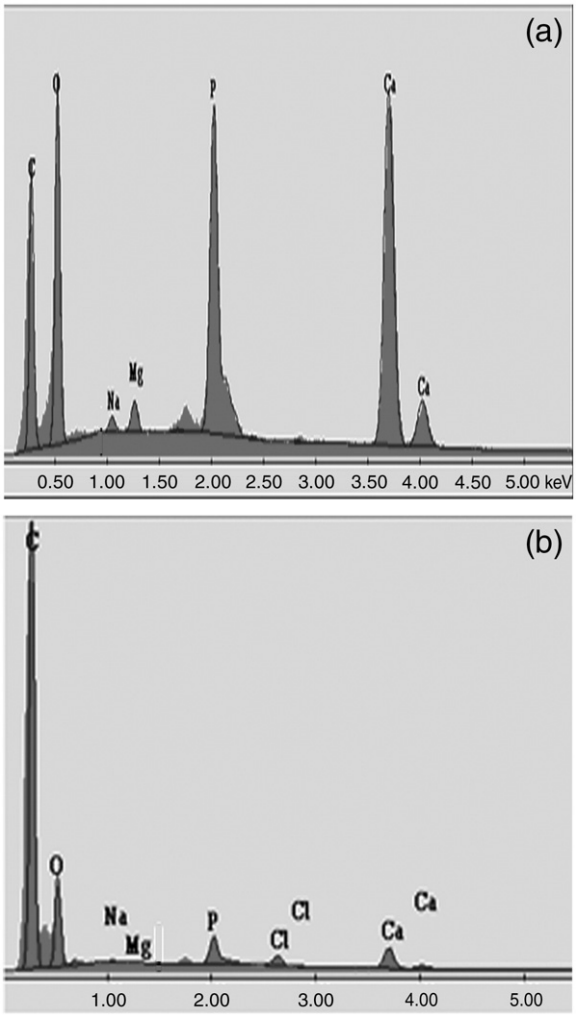

Fig. 6. Chemical analysis results obtained from the fracture surface of the turtle shell carapace; (a) bony layers and (b) inside of the closed-cell (fibers).

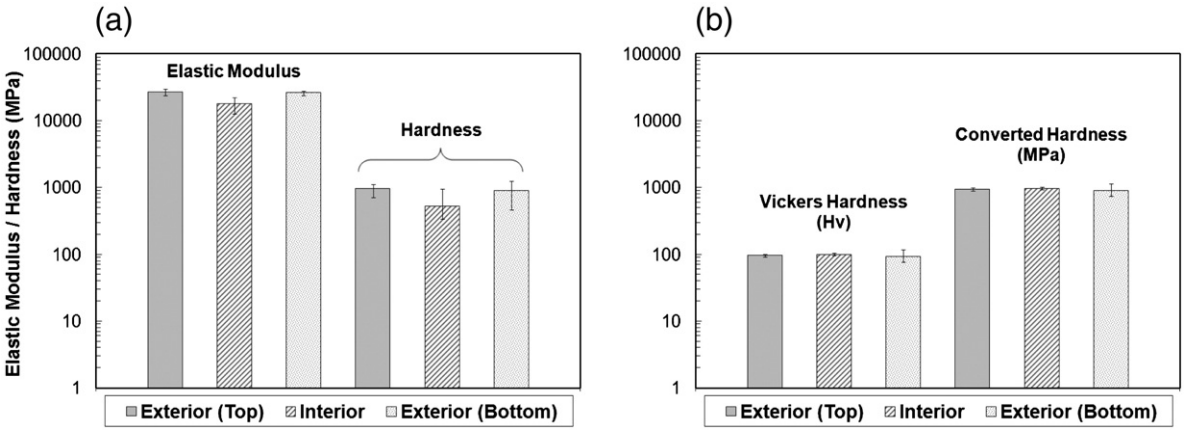

Fig. 7. Indentation test results obtained from (a) nano-indentation and (b) Vickers hardness tests on the side surface of the turtle shell carapace.

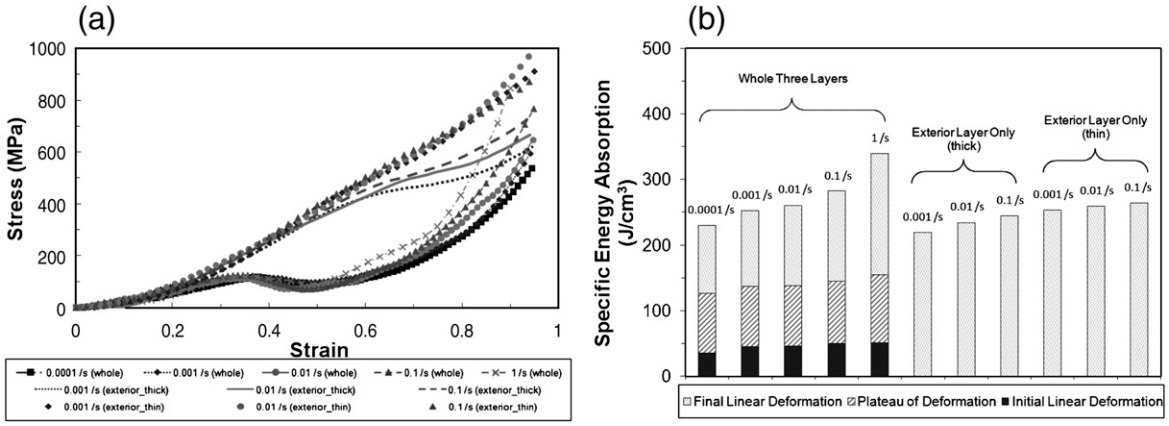

Fig. 8. Quasi-static compression test results on the turtle shell carapace coupon specimens under various strain rates and specimen geometries; (a) stress versus strain curves and (b) specific energy absorption as a function of density.

specimens can be extracted by fitting the test data into the following formulas:

$$\sigma_f = \frac{Mc}{I} = \left(\frac{FL}{4}\right)\left(\frac{d}{2}\right)\left(\frac{12}{bd^3}\right) = \frac{3FL}{2bd^2}, \varepsilon_f = \frac{6Dd}{L^2}, E_B = \frac{L^3 m}{4bd^3}$$

where, M is the maximum bending moment, c is the distance from center of specimen to the outer fibers, I is the moment of inertia of the cross-section, F is the applied load, L is the support span, d is the depth of test specimen, b is the width of test specimen, D is the maximum deflection of the specimen center, and m is the slope of the tangent to the initial straight line of the load deflection curve. Comparisons between three-point bending test results obtained from the experimental data and FEA simulations using ABAQUS software are depicted in Fig. 9 with the FEA simulation conditions listed in Table 1. The flexural stress versus strain curve showed a similar pattern to those obtained from the compression tests. Young's modulus, in this case, was determined by the slope of the initial linear elastic deformation curve. The FEA simulation results for a chosen actual test condition of $E_B = 7.1$ GPa are shown. The FEA simulations employed both single shell three-layer element and a discrete three-layer element in the region of initial elastic deformation. The E_B values

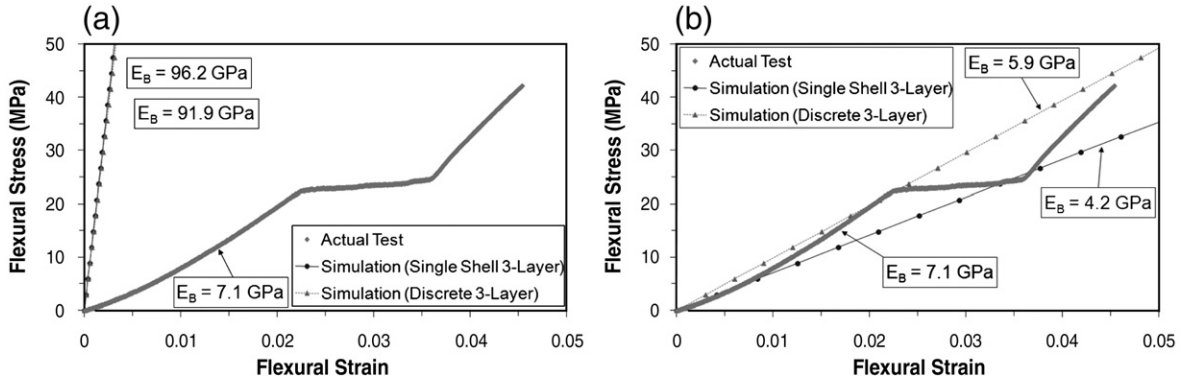

Fig. 9. Comparison of three-point bending test results obtained from actual data and ABAQUS finite element simulations; (a) without considering foam material effect, and (b) considering foam material effect.

Table 1
Finite element simulation conditions.

	Single shell three-layer	Discrete three-layer
Number of elements	2904	8712
Number of nodes	8505	19,811
Number of degrees of freedom	51,030	110,463

obtained from the initial simulations were much higher than that obtained from actual tests in both cases, since the material properties were measured without considering any effect from voids or pores in the outer shells as well as the inner core from the indentation tests. However, the exterior bone layer inevitably contained small voids, and the interior foam layer was basically a closed network of pores. Therefore, the FEA simulation results showed much stiffer stress versus strain responses than the experiments as shown in Fig. 9a. When the void volume fraction was considered, the FEA results showed much closer results as illustrated in Fig. 9b. Based on the void volume fraction in the turtle shell, the overall material properties could be estimated using an equivalent inclusion idealization and then adopted in the finite element model. By using modified material properties, the FEA simulation results gave better comparisons with experimental test results (Fig. 9b); the three-discrete layer approach captures strain reversal through-the-thickness direction if the soft core material is located between hard face sheet materials like a sandwich structure. However, one single shell element simulation through-the-thickness direction did not capture the strain reversal that occurred in the soft core material. For future studies, a better approximation of material properties for each component in the turtle shell needs to be developed for the FEA.

4. Conclusions

Several conclusions can be garnered from this study of the structure-property relations of a box turtle shell. The turtle shell carapace is a sandwich composite structure having denser exterior lamellar bone layers and an interior bony network of closed-cell fibrous foam layer. Although the textural morphology is different between the exterior layers and interior bony closed-cell walls, the comparable hardness and modulus values were essentially the same, ~1 GPa and ~20 GPa, respectively. Compression and flexure test results showed a typical nonlinear deformation behavior cognizant of man-made foams. As illustrated from finite element analyses simulations, the interior closed-cell foam layer plays a significant role on the overall deformation behavior of the turtle shell. The finite element simulations also showed comparable agreement with the actual experimental test data.

Acknowledgements

The authors would like to acknowledge the financial supports for this work from the Center for Advanced Vehicular Systems at Mississippi State University under grant CAVS Initiatives 190000–060803-021000 and the U.S. Department of Army (DOD) through grant TCN07173 07121203. They also thank G. Bae, R. Rieves, and A. Ramsay for their assistance in sample preparation and testing.

References

[1] M.A. Meyers, A.Y.M. Lin, Y. Seki, P.-Y. Chen, B.K. Kad, S. Bodde, JOM 58 (2006) 36.
[2] A.Y.M. Lin, M.A. Meyers, K.S. Vecchio, Mater. Sci. Eng., C 26 (2006) 1380.
[3] R. Menig, M.H. Meyers, M.A. Meyers, K.S. Vecchio, Mater. Sci. Eng., A 297 (2001) 203.
[4] R. Menig, M.H. Meyers, M.A. Meyers, K.S. Vecchio, Acta Mater. 48 (2000) 2383.
[5] D.R. Katti, S.M. Pradhan, K.S. Katti, Rev. Adv. Mater. Sci. 6 (2004) 162.
[6] K.S. Katti, D.R. Katti, Mater. Sci. Eng., C 26 (2006) 1317.
[7] D.R. Katti, K.S. Katti, J.M. Sopp, M. Sarikaya, Comput. Theor. Polym. Sci. 11 (2001) 397.
[8] K.S. Katti, D.R. Katti, S.M. Pradhan, A. Bhosle, J. Mater. Res. 20 (2005) 1097.
[9] K.S. Katti, B. Mohanty, D.R. Katti, J. Mater. Res. 21 (2006) 1237.
[10] B. Mohanty, K.S. Katti, D.R. Katti, D. Verma, J. Mater. Res. 21 (2006) 2045.
[11] K. Katti, D.R. Katti, J. Tang, S. Pradhan, M. Sarikaya, J. Mater. Sci. 40 (2005) 1749.
[12] F. Barthelat, C.-M. Li, C. Comi, H.D. Espinosa, J. Mater. Res. 21 (2006) 1977.
[13] T. Graham, M. Sarikaya, Mater. Sci. Eng., C 11 (2000) 145.
[14] E. DiMasi, M. Sarikaya, J. Mater. Res. 19 (2004) 1471.
[15] C. Sachs, H. Fabritius, D. Raabe, J. Struct. Biol. 155 (2006) 409.
[16] D. Raabe, P. Romano, C. Sachs, H. Fabritius, A. Al-Sawalmih, S.-B. Yi, G. Servos, H.G. Hartwig, Mater. Sci. Eng., A 421 (2006) 143.
[17] D. Raabe, C. Sachs, P. Romano, Acta Mater. 53 (2005) 4281.
[18] Y. Seki, B. Kad, D. Benson, M.A. Meyers, Mater. Sci. Eng., C 26 (2006) 1412.
[19] Y. Seki, M.S. Schneider, M.A. Meyers, Acta Mater. 53 (2005) 5281.
[20] A. Lin, M.A. Meyers, Mater. Sci. Eng., A 390 (2005) 27.
[21] K.S. Vecchio, JOM 57 (2005) 25.
[22] D.R. Katti, K.S. Katti, J. Mater. Sci. 36 (2001) 1411.
[23] D. Alderton, Turtles & Tortoises of the World, Facts on File, New York, New York, 1988.
[24] L.M. Ashley, Laboratory Anatomy of the Turtle, W.C. Brown Co., Dubuque, Iowa, 1955.
[25] A.F. Carr, Handbook of Turtles, Comstock Pub. Associates, Ithaca, New York, 1952.
[26] J.R. Vinson, The Behavior of Sandwich Structures of Isotropic and Composite Materials, Technomic Publishing Company, Lancaster, PA, 1999.
[27] T.E. Lacy, Y. Hwang, Compos. Struct. 61 (2003) 115.
[28] Y. Hwang, T.E. Lacy, J. Compos. Mater. 41 (2007) 367.
[29] L.J. Gibson, M.F. Ashby, Cellular Solids: Structure and Properties — Second Edition, Cambridge University Press, Cambridge, U.K., 1997.